TRENDS IN SCIENCES 2026; 23(4): 11897
https://doi.org/10.48048/tis.2026.11897 RESEARCH ARTICLE

Exploring the Antibacterial and Antioxidant Potentials of Nickel@Chitosan Nanocomposites

Khoirina Dwi Nugrahaningtyas[1,*], Eny Kusrini[2], Salwa Salsabila[1], Dina Fitriana[1], Triana Kusumaningsih[1], Fitria Rahmawati[1], Eddy Heraldy[1], Yuniawan Hidayat[1], I. F. Nurcahyo[1], Sri Juari Santoso[3] and Anwar Usman[4]

[1]*Department of Chemistry, Faculty of Mathematics and Natural Sciences, Sebelas Maret University, Jawa Tengah 57126, Indonesia*
[2]*Department of Chemical Engineering, Faculty of Engineering, Universitas Indonesia, Kampus Baru UI, Depok 16424, Indonesia*
[3]*Department of Chemistry, Faculty of Mathematics and Natural Sciences, Universitas Gadjah Mada, Yogyakarta 55281, Indonesia*
[4]*Department of Chemistry, Faculty of Science, Universiti Brunei Darussalam, Jalan Tungku Link BE1410, Brunei Darussalam*

([*]Corresponding author's e-mail: khoirinadwi@staff.uns.ac.id)

Received: 15 September 2025, Revised: 10 October 2025, Accepted: 17 October 2025, Published: 1 January 2026

Abstract

Nickel-based nanocomposites have become an interesting research subject for developing effective antimicrobial materials that address the global challenges of antibiotic resistance and oxidative stress. This study explored the bioactivity potential of nickel-based nanocomposites integrated into a chitosan (CS) matrix. The co-precipitation approach, incorporating Tween-20, sodium tripolyphosphate (STPP), and sodium hydroxide (NaOH), has been employed to manufacture Ni@CS nanocomposites. The antibacterial activity of the Ni@CS nanocomposite was determined using an agar well technique, while its antioxidant activity was rated based on its ability to reduce DPPH radicals. The formation of Ni@CS nanocomposites was validated by detecting Ni absorption and the NiO phase according to ICSD#61544. The antibacterial efficacy showed that Ni@CS-25 had a maximal inhibition zone of 26.11 mm against B. *cereus* ATCC 10556. Meanwhile, the Ni@CS nanocomposite showed antioxidant activity at a moderate IC_{50} level.

Keywords: Antibacterial, Antioxidant, Antiradical efficiency, Bioactivity, Chitosan, Concentration, IC_{50}, Nanocomposites

Introduction

The illnesses caused by gram-positive and gram-negative bacteria provide challenges for biomedical scientists [1]. Gram-positive bacteria, such as *Streptococcus pyogene*s, are known to cause throat infections, whereas *Bacillus cereus* has been associated with intestinal infections [2–4]. Gram-negative bacteria, including *Klebsiella pneumonia* and *Escherichia coli*, can cause respiratory and urinary tract infections [5,6]. Meanwhile, oxidative stress can lead to several health issues, including Alzheimer's, cardiovascular disease, cancer, and schizophrenia [7,8]. Novel antibacterial and antioxidant materials are needed to combat the global issues, including antimicrobial resistance and free radical damage. Nanotechnology may solve these issues by creating new materials for biomedicine and food technology [9,10]. In this context, nickel-based nanoparticles are prominent promising materials. In particular, nickel oxide (NiO) nanoparticles are non-toxic, chemically stable, and possess electro-optical properties. They can effectively minimize natural

pollutants, increase heat resistance, improve electrical conductivity, and can build complex compounds with various ligands [11]. Nickel metal has a wide range of applications, including its uses in electrodes, catalysts, magnetic recording, batteries, gas sensors, capacitors, biomedicine, and drug delivery [12–15]. Furthermore, NiO nanoparticles are effective in treating bloodstream infections and pneumonia [12–15]. They are more effective than erythromycin at combating *K. pneumoniae* and *Proteus vulgaris*. NiO nanoparticles outperform erythromycin against both *K. pneumoniae* and *P. vulgaris.* Meanwhile, the biodegradable [16,17], non-toxic [18,19], and biocompatible polymer chitosan also have antibacterial properties [20,21]. Combining nickel oxide with chitosan is expected to enhance antibacterial performance. For example, the chitosan-NiO composite has higher antibacterial activities compared to NiO nanoparticles alone against *E. coli* and *Staphylococcus aureus* [13,22].

The antibacterial mechanism of chitosan is due to the electrostatic interaction between polycationic chitosan molecules and negatively charged macromolecular residues on the cell surface. The interactions lead to disruption and leakage of the cell membrane. Meanwhile, oligomeric chitosan will penetrate the microorganism cells and inhibit their growth by prohibiting transcription from DNA [23]. On the other hand, metal ions can disrupt the cell membrane to form a cell inhibitor zone. According to previous literature, metal ions such as Ni^{2+} will interact with negatively charged cell membranes through electrostatic attraction. Once inside the cell, nickel ions react with sulfhydryl groups in the cell membrane, thereby damaging the activity of bacterial synthetase and ultimately leading to cell death [14,24]. Therefore, incorporating metal ions into chitosan can increase the antibacterial activity of nanocomposites. In addition to selecting the base materials, the synthesis method is also a critical factor in achieving nanocomposites with optimal performance. Therefore, integrating nickel into a chitosan matrix as a nanocomposite is promising for improving both antibacterial and antioxidant activities.

Researchers have extensively explored various methods for synthesizing nanocomposites. Co-precipitation is a process that has simple, low-cost, non-toxic, and stable steps. This approach also employs Tween-20 to preserve stability throughout the dilution step [25]. The addition of sodium tripolyphosphate (STPP) promotes particle size reduction, whereas the NaOH addition aims to adjust the pH of the solution [26,27]. The concentration of metal ions in the nanocomposite influences the properties and catalytic activity generated. For example, a previous study demonstrated that chitosan-Pd nanocomposites displayed increased palladium peak intensity and catalytic activity when the Pd content was raised from 5 to 10 and 15 wt%, respectively [23]. The effectiveness of nanocomposite synthesis is demonstrated by characterization results acquired using X-ray fluorescence (XRF), which identifies the nickel element content of the nanocomposite. The Fourier-transform infrared (FTIR) spectroscopy analysis of NiO nanocomposites reveals stretching vibrations of metal-oxygen bonds and functional groups of Ni@CS [15,28,29].

Meanwhile, X-ray diffraction (XRD) showed the presence of NiO nanocomposites with a face-centered cubic crystal structure according to JCPDS no. 47-1049. Scanning electron microscopy combined with energy-dispersive X-ray spectroscopy (SEM-EDX) was employed to examine the morphology and elemental composition of the nanocomposite [29]. After synthesis and characterization, the nanocomposites were evaluated for their antibacterial and antioxidant performance.

Previous studies reported that chitosan-NiO nanocomposites demonstrated stronger antibacterial activity than NiO nanoparticles and chitosan-MgO nanocomposites [13]. Our earlier studies also found that Ni@CS exhibited superior antibacterial activity compared to Cu@CS, Zn@CS, and Ag@CS [22]. However, the inhibition zone of Ni@CS in our previous work was smaller than that reported by Mizwari and colleagues [13]. This variance may be due to the lower concentration of Ni@CS (0.03 M) in our study compared with that (0.05 M) in their study. Consequently, this variation is assumed to be responsible for the difference in the size of the inhibition zone. Therefore, the purpose of this study was to look at how metal concentration affects antibacterial activity. Antibacterial tests were conducted against 4 bacterial strains: Gram-positive bacteria (*S. pyogenes* ATCC 19615 and *B. cereus* ATCC 10556) and Gram-negative

bacteria (*K. pneumoniae* ATCC 13883 and *E. coli* ATCC 25922).

In parallel, the antioxidant activity was assessed using the DPPH radical scavenging method, and the percentage of inhibition was used to determine the IC_{50} value [30]. The IC_{50} number represents the potential antioxidant needed to eliminate 50% of the radicals present. Understanding the role of nickel metal content in affecting the biological activity of nanocomposites may help researchers build more effective and sustainable antibacterial and antioxidant materials.

Overall, the aim of this study is to conduct a systematic investigation into various concentrations of nickel@chitosan (Ni@CS) and to assess their correlation with bioactivities, namely antibacterial and antioxidant. Furthermore, this research can provide a solid foundation for developing practical applications of nickel-based nanocomposites in various fields, including health and food.

Materials and methods

A commercial pharmaceutical-grade chitosan (deacetylation degree of 87.5%, Mr 501.5 g/mol), nickel acetate, polysorbate (Tween-20), and deionized water were purchased from UD Cahaya Labsain. Glacial acetic acid (CH_3COOH), methanol (CH_3OH), sodium hydroxide (NaOH), and sodium tripolyphosphate (STPP) with pro analysis grade were purchased from Merck. Meanwhile, reagent 1,1-diphenyl-2-picrylhydrazyl (DPPH) and ascorbic acid were purchased from Sigma-Aldrich.

Synthesis of nickel-chitosan nanocomposites

Nano-chitosan was prepared according to procedures reported in our previous study [22]. Nickel-chitosan nanocomposites were synthesized using the co-precipitation method [22,23,31]. The chitosan solution was made by dissolving 3.4 g of pure chitosan in 100 mL of 2% CH_3COOH. The chitosan solution was stirred for one hour and allowed to stand for 24 h. The chitosan solution was filtered, and the filtrate was added with 34 mL of Tween-20 dropwise. Into the solution, 0.0509 g of nickel acetate (5% by weight) was added, followed by 50 mL of 1.4 mM STPP. The solution was then stirred for 45 min.

Meanwhile, the pH of the solution was adjusted to the range of pH 6.5 - 6.8 with 1 M NaOH and stirred for one hour. The suspension formed was filtered and dried in an oven at 120 °C for 3 h. The dried solid, Ni@CS-5 nanocomposite, was collected and placed in a desiccator. A similar procedure was also carried out for other Ni@CS nanocomposites with various Ni concentrations, which were denoted as Ni@CS-10, Ni@CS-15, Ni@CS-20, and Ni@CS-25.

Characterization of nickel chitosan nanocomposites

Analysis of nanocomposite functional groups was carried out by recording the vibrational spectrum in the range of 400 - 4,000 cm^{-1} using an FTIR spectrophotometer (Shimadzu Prestige 21). The crystallinity properties of the nanocomposite were analyzed by observing the diffraction patterns recorded between 10° and 80° at a scanning speed of 2° 2θ min cm^{-1} using an XRD diffractometer (Shimadzu 700 maxima). The surface morphology of the nanocomposites was recorded using a SEM-EDX (Jeol JSM-IT200).

Antibacterial activity test

The antibacterial performance was evaluated using the well diffusion method, in accordance with procedures reported in literature [12,32], against gram-positive bacteria (*S. pyogenes*, *B. cereus*) and gram-negative bacteria (*K. pneumoniae*, *E. coli*). In this experiment, Ni@CS-5 nanocomposites were dissolved in 2% CH_3COOH. This antimicrobial test includes chloramphenicol as a positive control and acetic acid (2 %v/v) as a negative control. According to previous research, a 6 mm cork borer was used to create well holes in the medium [12]. The 2 to 4 wells were created to control the required test fluid. The wells were placed at an appropriate distance from one another and from the media's edge. Each 20 µL test solution was inserted into the well holes. The media was then allowed to stand for a few minutes, allowing the test solution to diffuse into the media. The test solution was then kept at 37 °C for 18 to 24 h. Then, the antibacterial performance was assessed using the media's cell inhibition zone (clear zone). A similar step was used on the Ni@CS-10, Ni@CS-15, Ni@CS-20, and Ni@CS-25 nanocomposites.

Antioxidant performance test

The antioxidant activity test was evaluated using the DPPH reagent, as previously published with minor changes [33]. The first step was dissolving 1 mg of DPPH in 10 mL of methanol to prepare a 100 ppm DPPH solution. The DPPH solution was homogenized in a flask coated with aluminum foil. The next step was to prepare a sample solution of 100 ppm, which was achieved by dissolving 0.5 mg of Ni@CS nanocomposites in 5 mL of methanol. From this solution, 5 concentrations of the sample solution (5, 10, 15, 20, and 25 ppm) were created by mixing 250 - 1,250 µL of the sample with the DPPH (100 ppm) solution to a final volume of 5 mL. Then the sample solutions were incubated in the dark for half an hour.

The UV-Vis spectrophotometer was used to monitor the radical scavenging activity of the Ni@CS-5 nanocomposites. Meanwhile, the methanol was used as a blank. The absorbance of the Ni@CS-5 nanocomposite solutions at 516.5 nm was measured on a UV-Vis double-beam spectrophotometer (Hitachi UH5300) [34,35]. This measurement was replicated up to 3 times at each sample concentration. Similar procedures were also performed on Ni@CS-10, Ni@CS-15, Ni@CS-20, and Ni@CS-25 nanocomposites. Ascorbic acid was used as a positive control, and DPPH was used as a negative control in this antioxidant test. The absorbance reduction of the DPPH solution in the presence of the antioxidant was measured and used to calculate the percentage of inhibition using Eq. (1), where A and B are the absorbance of ascorbic acid and the tested sample, respectively; see previous research by Flieger and coworkers [35].

$$Inhibition\ percentage = \frac{A-B}{A} \times 100 \quad (1)$$

The IC_{50} value, the sample concentration that can inhibit 50% of DPPH radicals, is calculated based on the linear regression equation plot of the percentage of inhibition against the sample concentration. Then, the IC_{50} value was used to determine the antioxidant activity as antiradical efficiency (AE), using Eq. (2) [36].

$$AE = \frac{1}{IC_{50}} \quad (2)$$

Results and discussion

Nickel-chitosan nanocomposite

The parent chitosan changes its color from white to pale white when it becomes nanochitosan. The color changes also occur in Ni@CS-5 to Ni@CS-25 nanocomposites. The color change can be caused by adding Tween-20, STPP, and NaOH to nanochitosan, which is also associated with adding nickel acetate to the Ni@CS nanocomposite. The amount of Ni also influences the difference in color from Ni@CS-5 to Ni@CS-25, which is increasingly dark green with the Ni content. The green color indicates that the nickel element embedded in the chitosan mat is due to the electrostatic interaction between chitosan and nickel ions. The parent chitosan, nanochitosan, and nickel-chitosan nanocomposites obtained in the form of dry solids are shown in **Figure 1**.

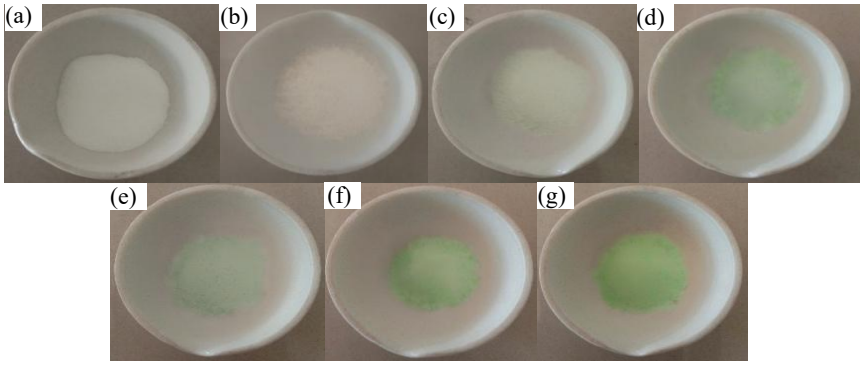

Figure 1 (a) parent chitosan, (b) nanochitosan, and nanocomposites of (c) Ni@CS-5, (d) Ni@CS-10, (e) Ni@CS-15, (f) Ni@CS-20, and also (g) Ni@CS-25.

Morphology of nickel-chitosan nanocomposites

Morphological analysis was performed to determine the shape, matrix, filler phases, and the presence of the Ni component in the nanocomposites using SEM-EDX (**Figure 2**). The SEM images suggested that nanochitosan has a smooth and slightly porous surface. Meanwhile, a morphological change was observed in the Ni@CS-5 to Ni@CS-25 nanocomposites, resulting in an irregular granular structure with a rough and porous surface. This morphology is composed of small spherical particles associated with nickel particles.

This morphological difference indicates the agglomeration of nickel particles within the chitosan matrix. Previous literature shows that increasing metal ion concentration can trigger agglomeration due to interparticle attractive forces [37,38]. This agglomeration produces larger particles formed from aggregations of nano-sized nickel particles. This is similar to the observations made with CS-ZnS and CS-TbS nanocomposites as reported by Kusrini *et al.* [39,40]. Furthermore, the formation of large agglomerates can also be attributed to the characteristics of NiO nanoparticles, which have high surface area and surface energy, following the previous publication [15].

Based on the observations, 2 phases can be identified in the nanocomposite structure: the chitosan matrix phase and the nickel filler phase (**Figure 2**). The results of EDX analysis also support this finding by showing the presence of Ni elements in the Ni@CS nanocomposites, which was not found in the nanochitosan.

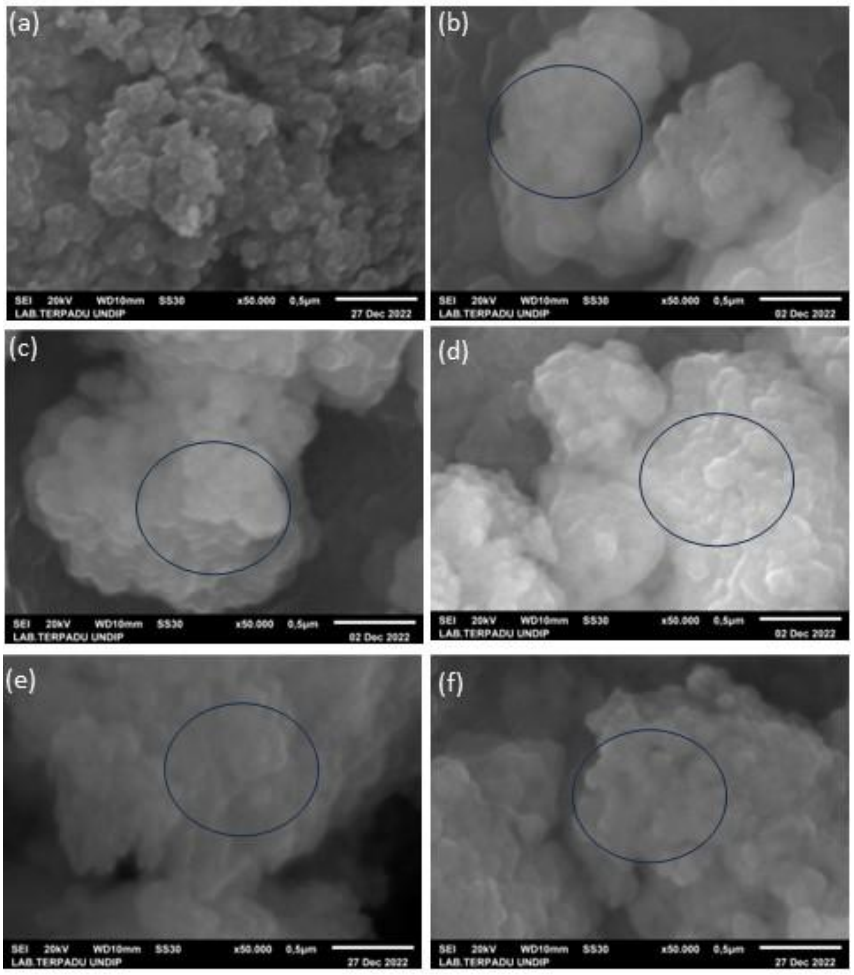

Figure 2 Morphology of (a) Nanochitosan and nanocomposites of (b) Ni@CS-5, (c) Ni@CS-10, (d) Ni@CS-15, (e) Ni@CS-20, and (f) Ni@CS-25, where the circles indicated the chitosan matrix phase and the nickel filler phase.

Functional groups of nickel-chitosan nanocomposites

Vibrational spectra of the Ni@CS nanocomposites were analyzed to determine the changes in functional groups of chitosan upon converting to nanochitosan and nickel-chitosan nanocomposites. Based on FTIR spectra shown in **Figure 3**, parent chitosan shows NH_2 twisting vibration at ~891 cm^{-1}, which is a typical vibration of chitosan, following the report by Nivethaa *et al.* [41]. Meanwhile, the absorption band of C–O stretching vibration at 1,081 cm^{-1} and bending vibrations of $–CH_3$ at 1,374 and 1,355 cm^{-1} are estimated to come from the acetyl group [20,31]. As reported in a previous publication, the 3 absorptions disappeared in nanochitosan. However, a new absorption appeared at 1,116 and approximately 921 cm^{-1}, which was associated with the presence of an unidentified compound and P–O from STPP [22]. The CH_2 vibrations are present at the bands of 1,473 and 1,461 cm^{-1} for parent chitosan and nanochitosan, respectively [23,41,42].

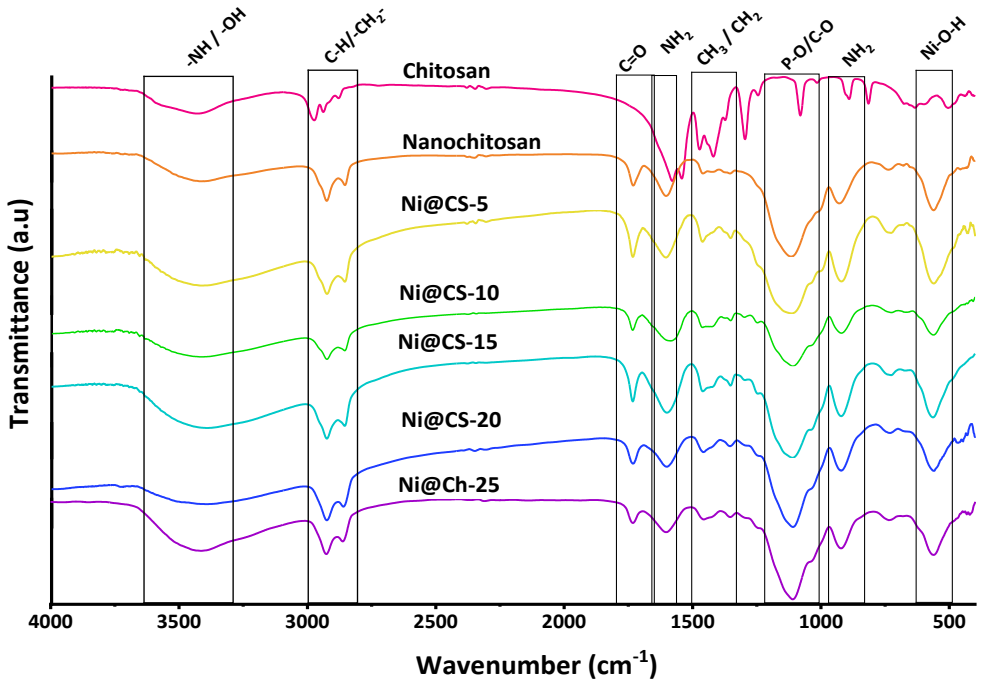

Figure 3 FTIR spectra of chitosan, nanochitosan, and nanocomposites of Ni@CS-5, Ni@CS-10, Ni@CS-15, Ni@CS-20, and Ni@CS-25.

Figure 3 also shows a peak at 1,604 cm^{-1}, which is associated with the NH_2 bending that occurs when the parent chitosan becomes nanochitosan [43]. Absorption at 1,732 cm^{-1} of nanochitosan indicates the presence of C=O [44]. The bands at 2,881, 2,856, 2,941, and 2,928 cm^{-1} indicate the presence of C–H stretching in both parent chitosan and nanochitosan [13,31]. Meanwhile, the absorption at the 3,429 and 3,418 cm^{-1} region in parent chitosan and nanochitosan is associated with O–H and N–H stretching [13,20,42]. The incorporation of Ni also impacts the appearance of bands of Ni@CS nanocomposites, such as Ni–O–H and Ni–O vibrations at ~561 and ~670 cm^{-1} [13,23]. The slight broadening of bands at ~921 and ~1,115 cm^{-1} suggests that the interaction of nickel metal with the nanocomposite involves $–NH_3^+$ and P–O groups [22]. Broadening of band in the region of ~1,353 and ~1,461 cm^{-1} is seen at all concentrations of Ni nanocomposites, led by disruption due to CH_3 and CH_2 bending in the nanocomposite [23,31].

According to previous publications, the Ni@CS nanocomposite's NH_2 bending absorption band grows in the 1,604 cm^{-1} region as the Ni content increases [43]. Meanwhile, similar to another researcher, our study found that the carbonyl group (C=O) interacts with the Ni@CS nanocomposite, resulting in a significant

absorption at around 1,734 cm^{-1} [41]. The C–H stretching increases from around 2,857 to roughly 2,927 cm^{-1} when the Ni concentration of the nanocomposite increases [13,31]. The Ni@CS nanocomposite also shows absorption in the ~3,418 cm^{-1} region, which can be linked to either O–H or N–H stretching [13,43]. The absorption bands are summarized in **Table 1**.

Table 1 FTIR absorption wavenumber data from samples and references.

Wavenumber (cm^{-1})							Reference [1,19,22,42,43]	Functional Group
CS	**Nano CS**	**Ni@CS-5**	**Ni@CS-10**	**Ni@CS-15**	**Ni@CS-20**	**Ni@CS-25**		
n.a.	n.a.	561	562	563	560.35	563	~500	$Ni–O–H_{Bending}$
n.a.	n.a.	727	725	727	731	735	~400 - 854	$Ni–O_{Bending}$
891	928	921	921	922	922	922	~895	$NH_{2\ twisting}$
1,081	1,116	1,114	1,110	1,111	1,110	1,109	~1,115 – 1,117	C–O/ P–O/P=O Bending
1,374	1,355	1,353	1,353	1,353	1,354	1,353	~1,381	CH_2/
1,473	1,461	1,461	1,461	1,461	1,460	1,456	~1,404	$CH_{3\ Bending}$
1,579	1,604	1,604	1,569	1,600	1,601	1,602	~1,600 - 1,674	$NH_{2\ Bending}$
2,881	2,856	2,856	2,857	2,857	2,862	2,862	~2,877 ~ 2,929	$C–H_{stretching}$
2,941	2,928	2,926	2,927	2,927	2,927	2,926		
3,429	3,418	3,418	3,418	3,380	3,394	3,413	~3,409 - 3,468	N–H/O–$H_{stretching}$

n.a.: Not available.

Structure of nickel-chitosan nanocomposites

Based on comparisons with those reported in previous research results [13,15,31,43], changes in chitosan into nanochitosan can be observed based on changes from crystalline into amorphous structure, as confirmed in **Figure 4**. Meanwhile, adding metal did not change the structure significantly. The intensity of the chitosan peak diminishes as the concentration of Ni in the nanocomposite increases, aligning with the literature [23,43]. The band intensity in the Ni@CS nanocomposite diminishes with minor broadening, attributable to the strain encountered by the metal and the nanocomposite's structure [15].

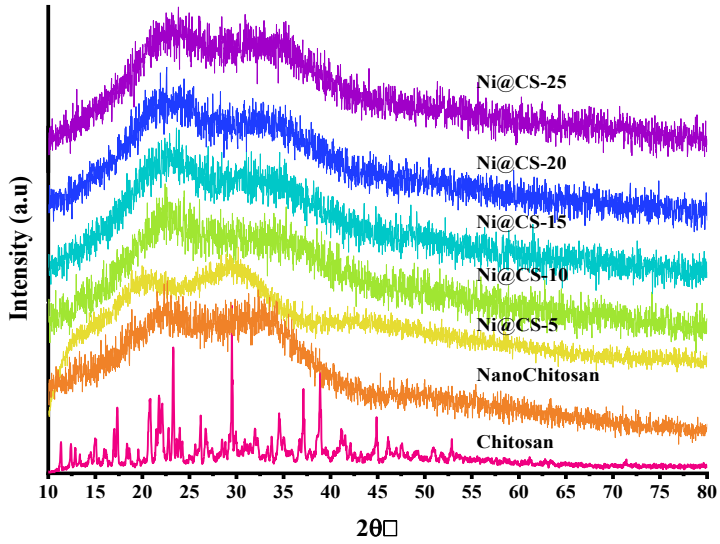

Figure 4 XRD pattern of chitosan, nanochitosan, and composites of Ni@CS-5, Ni@CS-10, Ni@CS-15, Ni@CS-20, and Ni@CS-25.

Further analysis also showed no new peaks, regardless of whether Ni metal was added or the concentration of Ni increased. Consequently, Rietica, an XRD data processing program, was used to analyze the nanocomposite's XRD data further (**Figure 5**). According to ICSD 61544, the refinement results indicate that the Ni@CS nanocomposite contains an NiO phase with a face-centered cubic crystal structure that is a member of the Fm3m space group. The Rietveld method was used to analyze the diffraction pattern data, providing statistical parameters to measure the fit between the observed data and the simulated/calculated patterns. These characteristics include the profile R-factor (Rp) and the weighted profile R-factor (Rwp). An Rp number less than 10 implies a good agreement between the experimental pattern and the standard-based simulation results, but an Rwp value less than 10 indicates satisfactory refinement quality. In this investigation, the obtained Rp and Rwp values were 6.05 and 7.82, indicating high confidence in the findings. According to Rahman *et al.* [14], these low Rp and Rwp values show that the observed diffraction pattern qualitatively corresponds to the anticipated crystal structure.

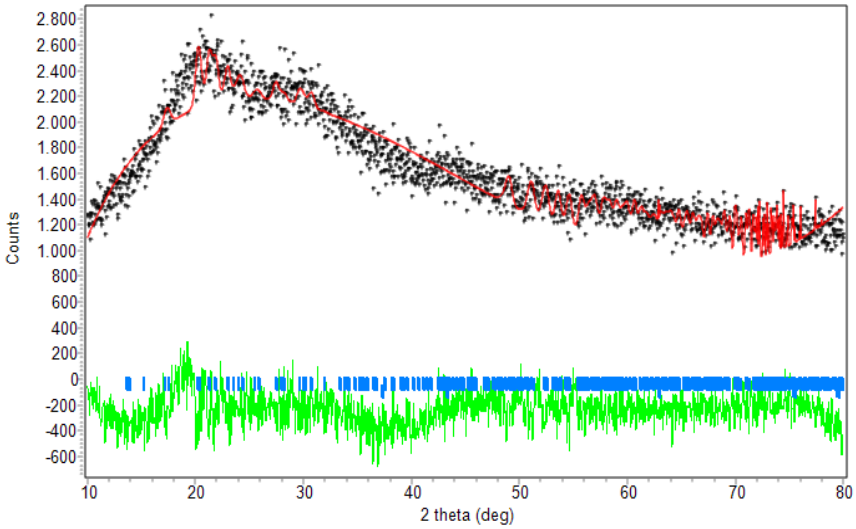

Figure 5 Refinement result of Ni@CS nanocomposite.

Antimicrobial performance of nickel-chitosan nanocomposites

The antibacterial performance test of the Ni@CS nanocomposite was conducted with careful consideration of every aspect. We used chloramphenicol as the positive control and acetic acid (CH_3COOH) at 2 V as the negative control. The test involved 4 species of bacteria: *K. pneumoniae* and *E. coli* as gram-negative bacteria. Then, *S. pyogenes* and *B. cereus* as gram-positive bacteria. Antibacterial performance of Ni@CS nanocomposites against 4 species of bacteria is presented in **Figures 5** - **8**.

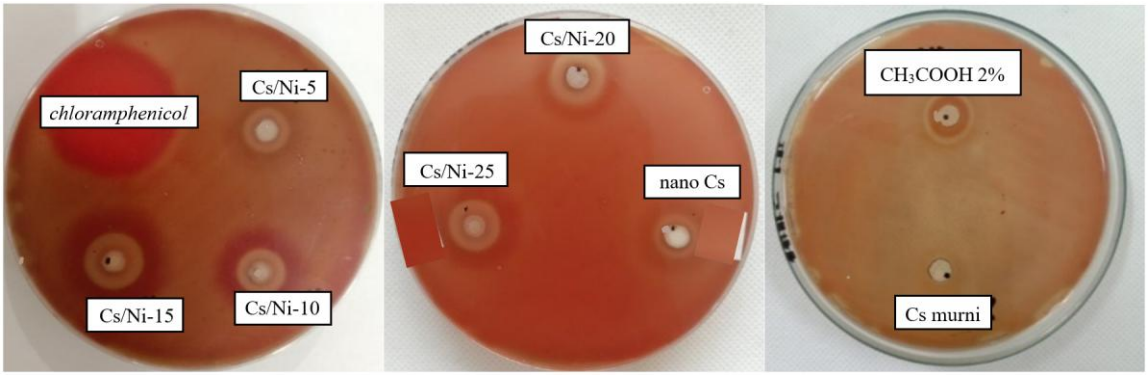

Figure 5 Antibacterial performance of chitosan, nanochitosan, Ni@CS-5 to Ni@CS-25 nanocomposites, positive control and negative control against *S. pyogenes* bacteria ATCC 19615.

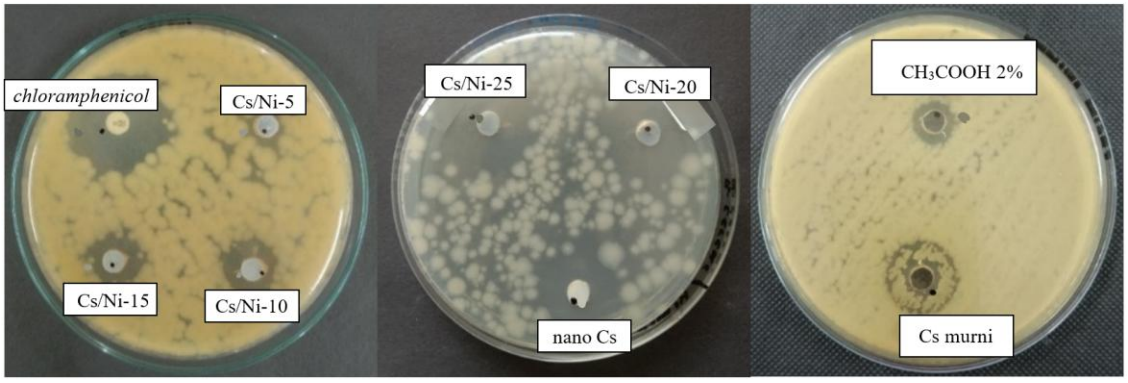

Figure 6 Antibacterial performance of chitosan, nanochitosan, Ni@CS-5 to Ni@CS-25 nanocomposites, positive control and negative control against B. Cereus bacteria ATCC 10556.

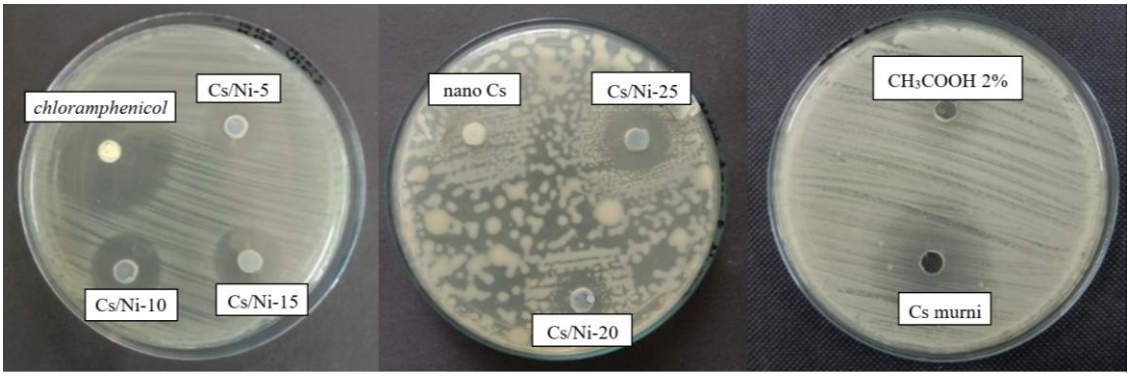

Figure 7 Antibacterial performance of chitosan, nanochitosan, Ni@CS-5 to Ni@CS-25 nanocomposites, positive control and negative control against *K. pneumoniae* bacteria ATCC 13883.

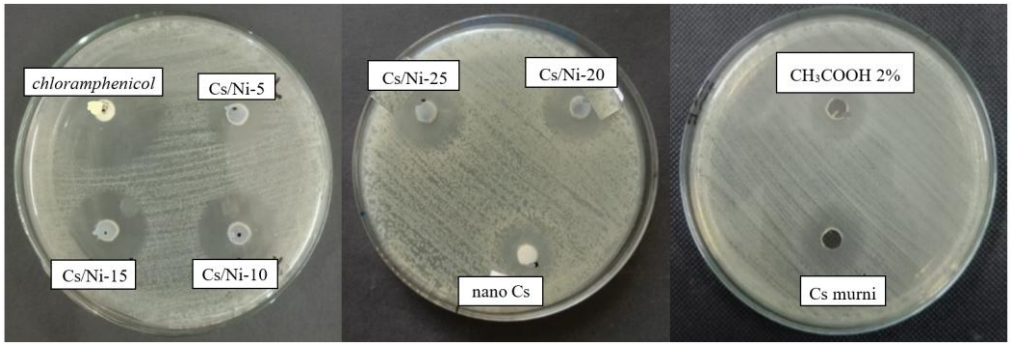

Figure 8 Antibacterial performance of chitosan, nanochitosan, Ni@CS-5 to Ni@CS-25 nanocomposites, positive control, and negative control against *E. coli* bacteria ATCC 25922.

Antibacterial gram-negative activity of nickel-chitosan nanocomposites

The Ni@CS-10 nanocomposites exhibited the highest antibacterial activity against both *K. pneumoniae* and *E. coli* (**Figure 9**). Meanwhile, chitosan exhibited no antibacterial activity against both types of bacteria, whereas chitosan nanoparticles only had an inhibition zone against *E. coli*. The test results showed that Ni@CS nanocomposites were more effective as antibacterial agents against *E. coli* than *K. pneumoniae*. This investigation found that the antibacterial efficacy against *E. coli* of Ni@CS is tenfold higher than that reported by Razon [45]. The antibacterial efficacy against *E. coli* of Ni@CS is slightly higher than those of Cu@CS, Zn@CS, and Ag@CS reported in our previous study [22], ganyong starch edible films, such as those reported by Silvia *et al.* [46], and also Ag/ZnO, which was obtained by Jha *et al.* [47]. Unfortunately, the antibacterial efficacy of Ni@CS, measured at 20.5 mm against *E. coli*, is lower than that of the chitosan-ZnO@gallic-acid film, which demonstrates an efficacy of 28 mm, as reported by Yadav *et al.* [48]. It is also slightly lower than the chitosan-dialdehyde cellulose composite film, which exhibited an efficacy of 22.37 mm in the study done by Qian *et al.* [49]. The disparity in antibacterial efficacy may be due to much lower amount of Ni@CS nanocomposites, as antibacterial agents, applied in the tests, which is just one-fifth of the ones utilized in the other previous studies.

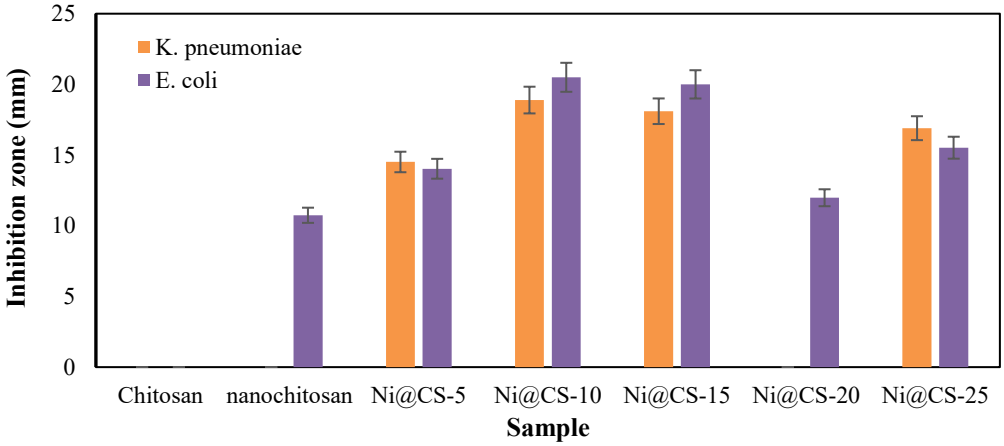

Figure 9 Antibacterial performance against gram-negative bacteria.

Antibacterial gram-positive activity of nickel-chitosan nanocomposites

The results showed that chitosan and nanochitosan could inhibit the growth of gram-positive bacteria, with *B. cereus* being better than *S. pyogenes* bacteria (**Figure 10**). However, adding nickel at a low percentage reduced its antibacterial performance. The antibacterial activity of Ni@CS nanocomposites increased as the percentage of nickel metal increased, with optimum inhibitory power for *S. pyogenes* occurring in the

Ni@CS-15 nanocomposite. Meanwhile, the Ni@CS-25 nanocomposite had the highest inhibition zone against *B. cereus*, which was 26.11 mm. Again, our investigation found that the antibacterial efficacy of Ni@CS is ten times superior to that reported by Razon [45], and chitosan/glutaraldehyde, as result study by Masfufah *et al.* [50]. The antibacterial efficacy of Ni@CS is also slightly superior to that of Cu@CS, Zn@CS, and Ag@CS in our previous study [22], and ganyong starch edible films such reported by Silvia *et al.* [46].

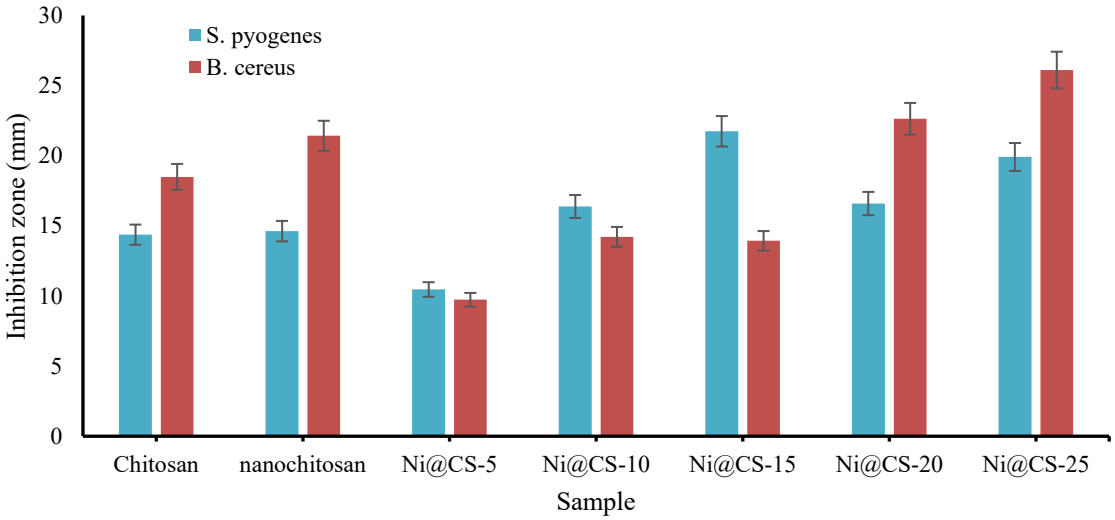

Figure 10 Antibacterial performance against Gram-positive bacteria.

Previous research suggests that antibacterial activity can be attributed to chitosan's protonated amino group ($-NH_3^+$), which binds to carboxyl and phosphate groups on the bacterial surface and damages the outer membrane structure. As a result, metal ions such as Ni^{2+} are liberated, interacting with the positively charged cell membrane. This interaction attracts the 2 charges and allows metal ions to enter the bacterial cell. Metal ions interact with sulfhydryl groups and phosphorus-containing substances within the bacterial cell membrane. This interaction hampers DNA replication. Additionally, the liberated metal ions attach to proteins in cells. This denaturation, such as synthesis activity in bacteria, significantly limits their capacity to develop through cell division, eventually leading to bacterial mortality [13,14].

The antibacterial activity of the Ni@CS nanocomposite is superior to that of the parent chitosan or nanochitosan due to a combination of mechanistic activities that the Ni@CS nanocomposite possesses, including bacterial cell disruption by the positively charged chitosan [13]. A previous study reveals that chitosan's strong chelation with bacterial cell walls might improve lipophilic behavior. The interaction of the cell membrane and metal ions can also inhibit bacterial cell development [13].

In general, the Ni@CS nanocomposites exhibit greater bacterial inhibitory effect against Gram-positive bacteria than against Gram-negative bacteria, due to variations in cell membrane structure and microbial composition. Gram-positive bacteria are more sensitive to surface injury than Gram-negative bacteria due to their single cytoplasmic membrane [13]. The researchers also discovered that the Ni@CS nanocomposite possesses antibacterial activity that varies with Ni concentration. This discovery aligns with previous research, which found that the metal ion amount of the nanocomposite causes antibacterial activity against pathogenic microorganisms [23].

Antioxidant performance of nickel chitosan nanocomposites

The color change seen when DPPH is introduced to the Ni@CS nanocomposite (**Figure 11**) indicates antioxidant activity, with the degree of purple color shift regulated by antioxidant strength [35,51–54]. This color

shift is caused by the reduction process in DPPH, which causes the purple complex to disappear [35]. The absorption values of the test and control solutions were used to calculate the inhibition value (IC_{50}), which was the foundation for determining the antioxidant activity of the Ni@CS nanocomposites. When ascorbic acid is used as a positive control, the color of DPPH shifts from dark purple to clear. Our investigation found that the dark purple diminishes gradually as the Ni ion concentration decreases, yet it stays purplish.

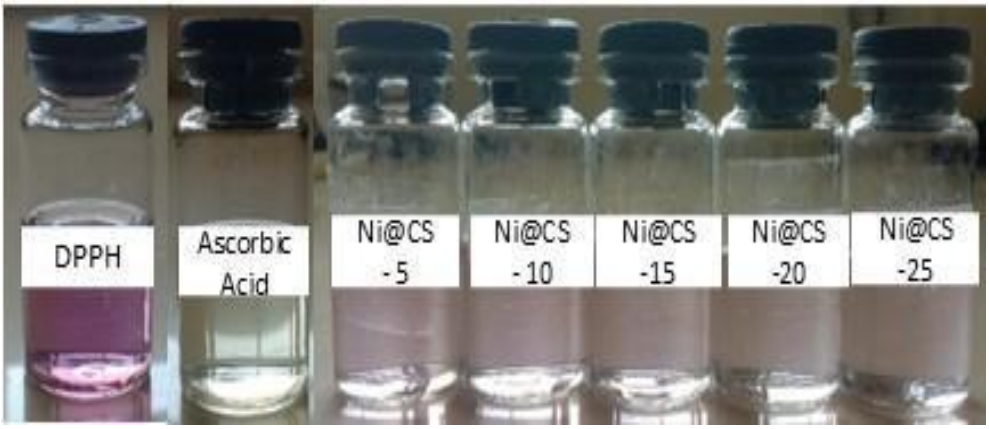

Figure 11 Antioxidant performance of DPPH, ascorbic acid, and nickel chitosan nanocomposites.

Several studies have examined the mechanism by which chitosan suppresses free radicals. The interaction of the DPPH radical and the free amino group ($–NH_2$) on the chitosan chain forms a stable macromolecular radical. The amino groups can absorb hydrogen ions from the solution, forming an ammonium group ($–NH_3^+$) [36,55]. Kusrini *et al.* [56] reported similar observations for iron-oxide chitosan/samarium/ranitidine microparticles. Schreiber *et al.*[57] discovered that pure chitosan with 80% deacetylation had only a 9.4% inhibitory activity against DPPH radicals at dosages ranging from 250 to 5,000 µg/mL, indicating its limited ability to suppress free radicals. Similarly, Mahae and colleagues [36], discovered that chitosan has low antioxidant activity, with an IC_{50} value greater than 500 µg/mL. Meanwhile, the inhibition percentage of Ni@CS nanocomposites at nickel concentrations of 5 - 25 ppm ranged from 13% to 35% (**Supplementary Material**). Therefore, it is possible to infer that the antioxidant activity of purified chitosan and Ni@CS nanocomposites is influenced by the concentration and presence of nickel ions. Despite this, the antioxidant activity of Ni@CS nanocomposites is not as high as that of the positive control. The antioxidant activity of both the positive control and test samples grew in percentage inhibition as the quantity of the test samples increased, especially between 250 and 1,250 µg/mL, where the percentage inhibition of the positive control ranged from 20% to 99%.

Based on the observed percentage of inhibition, the IC_{50} value and antiradical efficiency (AE) were calculated. Jumina *et al.* [58] classified antioxidant activity based on IC_{50} values as forceful (IC_{50} < 50 µg/mL), strong (50 - 100 µg/mL), moderate (101 - 250 µg/mL), and weak (250 - 500 µg/mL). Thereby, chitosan with an IC_{50} value above 500 µg/mL is considered to have weak antioxidant activity. The study results show that adding nickel (Ni) improves antioxidant efficacy (**Table 2**). However, it is important to highlight that a larger nickel ratio in chitosan reduces antioxidant efficacy, which contradicts the findings reported by Desai and colleagues [59]. Interestingly, Ni@CS samples showed enhanced antioxidant activity relative to Cu@CS samples, which are acknowledged as anticancer agents with an IC_{50} value of 206 µg/mL, as reported by Sun and coworkers [60]. Ni@CS is also superior to ZnO quantum dots-chitosan biocomposite, as found by Shu *et al.* [61], the chitosan-ZnO@gallic-acid film that was reported by Yadav and colleagues [48], and microcapsules of *T. diversifolia* leaves plant extract which found by Alymayda *et al.* [62].

Table 2 IC_{50} classification and antioxidant efficiency of samples.

Sample	IC_{50} (µg/mL)	AE	IC_{50} Classification [58]
Ascorbic acid	9.244	0.11	Very strong
Chitosan	$2.1\times10^{9*}$	4.76×10^{-10}	Very weak
Ni@CS-5	115.420	0.009	moderate
Ni@CS-10	143.327	0.007	moderate
Ni@CS-15	151.873	0.007	moderate
Ni@CS-20	171.319	0.006	moderate
Ni@CS-25	194.854	0.005	moderate

*Cited from Mahae and colleagues [36].

Conclusions

Overall, Ni@CS nanocomposites were successfully synthesized through the co-precipitation method with structural characteristics indicative of the Ni–O bond formation, due to the interaction between Ni and chitosan. Additionally, there was an enhancement in antimicrobial and antioxidant activities, confirming their potential as a multifunctional material. The novelty of this research lies in the study of the impact of Ni ion integration in the chitosan matrix, which can increase bioactivity. However, the research is still limited to *in vitro* tests and has not included aspects of toxicity or biocompatibility. In the future, the development of Ni@CS can be directed at biomedical applications, such as wound dressings or antimicrobial coatings on medical devices, as well as in the food industry as active packaging to inhibit microbial contamination and oxidation.

Acknowledgements

The authors are grateful to the Legal Entity State Funding Assistance (BPPTNBH) under the Indonesian Collaboration Research Program (RKI) Scheme C [Decision Letter No. 624/UN27/HK/2022 and Contract No. 872.1/UN27.22/PT.01.03/2022] and Sebelas Maret University for funding this research through Penguatan Kapasitas Grup Riset (PKGR-UNS) A with contract number 371/UN27.22/PT.01.03/2025.

Declaration of Generative AI in Scientific Writing

The author claims that AI was only used to enhance the writing and make it more fluid in this manuscript.

CRediT Author Statement

Khoirina Dwi Nugrahaningtyas: Conceptualization; Methodology; Writing - Original Draft; Software. **Salwa Salsabila:** Visualization; Investigation. **Dina Fitriana:** Investigation, **Triana Kusumaningsih:** Methodology. **Fitria Rahmawati:** Writing - Review & Editing. **Eddy Heraldy**: Writing - Review & Editing. **Yuniawan Hidayat:** Software, Validation, Writing - Review & Editing. **IF Nurcahyo:** Formal analysis. **Eny Kusrini:** Writing - Review & Editing, **Sri Juari Santoso:** Writing - Review & Editing. **Anwar Usman:** Writing - Review & Editing.

References

[1] MA Abureesh, AA Oladipo, ZM Mizwari and E Berksel. Engineered mixed oxide-based polymeric composites for enhanced antimicrobial activity and sustained release of antiretroviral drug. *International Journal of Biological Macromolecules* 2018; **116**, 417-425.

[2] NJ Avire, H Whiley and K Ross. A review of *Streptococcus pyogenes*: Public health risk factors, prevention and control. *Pathogens* 2021; **10(2)**, 248.

[3] R Dietrich, N Jessberger, M Ehling-Schulz, E Märtlbauer and PE Granum. The food poisoning toxins of *Bacillus cereus. Toxins* 2021; **13(2)**, 98.

[4] Y Wei, L Lei, H Jiang, Q Du, D Liu, L Chen, X Shi, Y Wang, J Li, Y Hu, X Xia and J Tu. Antibacterial and antibiofilm activities and mechanisms of *Toona sinensis* extracts against *Bacillus cereus* and its application in milk. *Current Research in Food Science* 2025; **10**, 101045.

[5] S Asokan, T Jacob, J Jacob, AA AlSosowaa, T Cherian, WJGM Peijnenburg and S Vijayan. *Klebsiella pneumoniae*: A growing threat in the era of antimicrobial resistance. *The Microbe* 2025; **7**, 100333.

[6] G Giuliano, G Hankache, M Sambo, MG Cusi, PE Lazzerini, L Gennari, M Fabbiani, F Montagnani and M Tumbarello. Urinary tract infections caused by Gram-negative bacteria in elderly hospitalized patients: Epidemiology, clinical features and outcomes in the era of antimicrobial resistance. *Journal of Global Antimicrobial Resistance* 2025; **44**, 116-126.

[7] E Cecerska-Heryć, A Polikowska, N Serwin, M Roszak, B Grygorcewicz, R Heryć, A Michalczyk and B Dołęgowska. Importance of oxidative stress in the pathogenesis, diagnosis, and monitoring of patients with neuropsychiatric disorders, a review. *Neurochemistry International* 2022; **153**, 105269.

[8] KR Aran and S Singh. Mitochondrial dysfunction and oxidative stress in Alzheimer's disease - A step towards mitochondria based therapeutic strategies. *Aging and Health Research* 2023; **3(4)**, 100169.

[9] SA Jasim, NMLA Maimuri, A Hashim, MH Abbas, A Hadi and H Ibrahim. Fabrication and enhancing the features of chitosan/SnO_2-ZnO nanocomposites films for optoelectronics and biological applications. *Trends in Sciences* 2025; **22(10)**, 10534.

[10] GG Ali, AZ Khalil and OA Alhamd. Growth and characterization of cadmium and nickel nanocomposites on porous silicon for some antibacterial properties. *Trends in Sciences* 2025; **22(8)**, 10054.

[11] K Subashini, S Prakash and V Sujatha. Biological applications of green synthesized zinc oxide and nickel oxide nanoparticles mediated poly(glutaric acid-co-ethylene glycol-co-acrylic acid) polymer nanocomposites. *Inorganic Chemistry Communications* 2022; **139**, 109314.

[12] S Anitha, M Suganya, D Prabha, J Srivind, S Balamurugan and ARR Balu. Synthesis and characterization of NiO-CdO composite materials towards photoconductive and antibacterial applications. *Materials Chemistry and Physics* 2018; **11**, 88-96.

[13] ZM Mizwari, AA Oladipo and E Yilmaz. Chitosan/metal oxide nanocomposites: synthesis, characterization, and antibacterial activity. *International Journal of Polymeric Materials and Polymeric Biomaterials* 2021; **70**, 383-391.

[14] MA Rahman, R Radhakrishnan and R Gopalakrishnan. Structural, optical, magnetic and antibacterial properties of Nd doped NiO nanoparticles prepared by co-precipitation method. *Journal of Alloys and Compounds* 2018; **742**, 421-429.

[15] BS Rathore, NPS Chauhan, S Jadoun, SC Ameta and R Ameta. Synthesis and characterization of chitosan-polyaniline-nickel (II) oxide nanocomposite. *Journal of Molecular Structure* 2021; **1242**, 130750.

[16] MSB Reddy, D Ponnamma, R Choudhary and KK Sadasivuni. A comparative review of natural and synthetic biopolymer composite scaffolds. *Polymers* 2021; **13(7)**, 1105.

[17] E Salehi, P Daraei and AA Shamsabadi. A review on chitosan-based adsorptive membranes. *Carbohydrate Polymers* 2016; **152**, 419-432.

[18] E Al-Abbad and F Alakhras. Removal of dye acid red 1 from aqueous solutions using chitosan-iso-vanillin sorbent material, *Indonesian Journal of Science and Technology* 2020; **5**, 352-365.

[19] A Anitha, VG Deepagan, VVD Rani, D Menon, SV Nair and R Jayakumar. Preparation, characterization, *in vitro* drug release and biological studies of curcumin loaded dextran sulphate-chitosan nanoparticles. *Carbohydrate Polymers* 2011; **84**, 1158-1164.

[20] LA Haruna, A Fristiohady, P Masrinoul, J Komaikul, K Ketsuwan and R Asasutjarit. Ganciclovir-loaded chitosan nanoparticles and their activity against HSV-1 inducing herpetic

retinitis. *Indonesian Journal of Science and Technology* 2025; **10**, 171-190.

[21] G Yuan, X Chen and D Li. Chitosan films and coatings containing essential oils: The antioxidant and antimicrobial activity, and application in food systems. *Food Research International* 2016; **89**, 117-128.

[22] KD Nugrahaningtyas, E Kusrini, S Salsabila, D Fitriana, A Usman, T Kusumaningsih and SJ Santoso. Synthesis of transition metal-nanochitosan composites using Ni, Cu, Zn, and Ag metal ions and applications as antibacterial agents. *International Journal of Technology* 2025; **16(1)**, 207-220.

[23] S Dhanavel, N Manivannan, N Mathivanan, VK Gupta, V Narayanan and A Stephen. Preparation and characterization of cross-linked chitosan/palladium nanocomposites for catalytic and antibacterial activity. *Journal of Molecular Liquids* 2018; **257**, 32-41.

[24] B Das, S Moumita, S Ghosh, MI Khan, D Indira, R Jayabalan, SK Tripathy, A Mishra and P Balasubramanian. Biosynthesis of magnesium oxide (MgO) nanoflakes by using leaf extract of *Bauhinia purpurea* and evaluation of its antibacterial property against *Staphylococcus aureus*. *Materials Science and Engineering: C* 2018; **91**, 436-444.

[25] SM Bashir, G Ahmed Rather, A Patrício, Z Haq, AA Sheikh, MZ ul Haq Shah, H Singh, AA Khan, S Imtiyaz, SB Ahmad, S Nabi, R Rakhshan, S Hassan and P Fonte. Chitosan nanoparticles: A versatile platform for biomedical applications. *Materials* 2022; **15(19)**, 6521.

[26] F Hu, PR Zou, F Zhang, K Thakur, MR Khan, R Busquets, JG Zhang and ZJ Wei. Wheat gluten proteins phosphorylated with sodium tripolyphosphate: Changes in structure to improve functional properties for expanding applications. *Current Research in Food Science* 2022; **5**, 1342-1351.

[27] Y Poureghbal, M Rahimi and M Akbari. Ionic gelation of chitosan with sodium tripolyphosphate using a novel combined nebulizer and falling film system. *The Canadian Journal of Chemical Engineering* 2022; **100(7)**, 1547-1557.

[28] R Nasiri, N Arsalani and Y Panahian. One-pot synthesis of novel magnetic 3-dimensional graphene/chitosan/nickel ferrite nanocomposite for lead ions removal from aqueous solution: RSM modelling design. *Journal of Cleaner Production* 2018; **201**, 507-515.

[29] S Yadav, J Yadav, M Kumar and K Saini. Synthesis and characterization of nickel oxide/cobalt oxide nanocomposite for effective degradation of methylene blue and their comparative electrochemical study as electrode material for supercapacitor application. *International Journal of Hydrogen Energy* 2022; **47**, 41684-41697.

[30] SM Nezhad, SA Pourmousavi, EN Zare, G Heidari, S Hosseini and M Peyvandtalab. Magnetic poly(1,8-diaminonaphthalene)-nickel nanocatalyst for the synthesis of antioxidant and antibacterial isoxazole-5(4H)-ones derivatives. *Heliyon* 2023; **9(5)**, e15886.

[31] E Kusrini, SN Paramesti, A Zulys, NZA Daud, A Usman, LD Wilson and N Sofyan. Kinetics, isotherm, thermodynamic and bioperformance of defluoridation of water using praseodymium-modified chitosan. *Journal of Environmental Chemical Engineering* 2019; **7(6)**, 103498.

[32] H Ali, TM Tiama and AM Ismail. New and efficient NiO/chitosan/polyvinyl alcohol nanocomposites as antibacterial and dye adsorptive films. *International Journal of Biological Macromolecules* 2021; **186**, 278-288.

[33] FMT Supriyanti, D Roslina, Z Zackiyah and I Hanifa. Strawberry-fortified yogurt: Production, sensory, antioxidant activity test, and model for practicum. *Indonesian Journal of Science and Technology* 2022; **7**, 551-564.

[34] MSO Alhar, D Muhammad, K Tahir, MEA Zaki, M Urooj, S Nazir, K Albalawi, HS Al-Shehri, EAM Saleh and AU Khan. An eco-benign biomimetic approach for the synthesis of Ni/ZnO nanocomposite: Photocatalytic and antioxidant activities. *Molecules* 2023; **28**, 1705.

[35] J Flieger, W Flieger, J Baj and R Maciejewski. Antioxidants: Classification, natural sources, activity/capacity measurements, and usefulness for the synthesis of nanoparticles. *Materials* 2021; **14(15)**, 4135.

[36] N Mahae, C Chalat and P Muhamud. Antioxidant and antimicrobial properties of chitosan-sugar complex. *International Food Research Journal* 2011; **18(4)**, 1543-1551.

[37] JZ Kuang, Y Yang, Z Zou, W Yuan, Z Huang and H Cheng. Effect of metal ions on the dispersion and agglomeration behavior of micro-fine wolframite. *Colloids and Surfaces A: Physicochemical and Engineering Aspects* 2022; **643**, 128747.

[38] H Wang, X Zhao, X Han, Z Tang, S Liu, W Guo, C Deng, Q Guo, H Wang, F Wu, X Meng and JP Giesy. Effects of monovalent and divalent metal cations on the aggregation and suspension of Fe_3O_4 magnetic nanoparticles in aqueous solution. *Science of the Total Environment* 2017; **586**, 817-826.

[39] E Kusrini, AI Safira, A Usman, EA Prasetyanto, KD Nugrahaningtyas, SJ Santosa and LD Wilson. Nanocomposites of terbium sulfide nanoparticles with a chitosan capping agent for antibacterial applications. *Journal Of Composites Science* 2023; **7(1)**, 39.

[40] E Kusrini, LD Wilson, KM Padmosoedarso, DP Mawarni, M Sufyan and A Usman. Synthesis of chitosan capped zinc sulphide nanoparticle composites as an antibacterial agent for liquid handwash disinfectant applications. *Journal of Composites Science* 2023; **7**, 52.

[41] EAK Nivethaa, S Dhanavel, A Rebekah, V Narayanan and A Stephen. A comparative study of 5-Fluorouracil release from chitosan/silver and chitosan/silver/MWCNT nanocomposites and their cytotoxicity towards MCF-7. *Materials Science and Engineering: C* 2016; **66**, 244-250.

[42] MAA Ab Rahman, SFS Mohamad and S Mohamad. Development and characterization of bio-composite films made from bacterial cellulose derived from oil palm frond juice fermentation, chitosan and glycerol. *Trends in Sciences* 2023; **20(8)**, 4919.

[43] S Dhanavel, EAK Nivethaa, V Narayanan and A Stephen. *In vitro* cytotoxicity study of dual drug loaded chitosan/palladium nanocomposite towards HT-29 cancer cells. *Materials Science and Engineering: C* 2017; **75**, 1399-1410.

[44] EAK Nivethaa, S Dhanavel, V Narayanan and A Stephen. Fabrication of chitosan/MWCNT nanocomposite as a carrier for 5-fluorouracil and a study of the cytotoxicity of 5-fluorouracil encapsulated nanocomposite towards MCF-7. *Polymer Bulletin* 2016; **73**, 3221-3236.

[45] BC Razon. Soft coral epibiotic bacteria *Vibrio alginolyticus* from Sarangani Bay, Mindanao, the Philippines as Potent Source of Antibacterial Agent. *Indonesian Journal of Science and Technology* 2024; **201**, 747-758.

[46] D Silvia, Z Zulkarnain, RI Fadhilah, H Kamilah and NNAK Shah. Effect of ginger (*Zingiber officinale*) extracts on mechanical and antimicrobial properties of ganyong starch edible films as primary packaging of crabstick. *Trends in Sciences* 2024; **21(7)**, 7711.

[47] PK Jha, C Chawengkijwanich, C Pokum, P Soisan and K Techato. Antibacterial activities of biosynthesized zinc oxide nanoparticles and silver-zinc oxide nanocomposites using *Camellia sinensis* leaf extract. *Trends in Sciences* 2024; **20(3)**, 5649.

[48] S Yadav, GK Mehrotra and PK Dutta. Chitosan based ZnO nanoparticles loaded gallic-acid films for active food packaging. *Food Chemistry* 2021; **334**, 127605.

[49] L Qian, R Jia, Q Zhao, N Sun, J Yang, J Wen, H Li, J Yang, L Mo, W Gao, S Deng and Z Qin. Tough, antibacterial, and antioxidant chitosan-based composite films enhanced with proanthocyanidin and carvacrol essential oil for fruit preservation. *Food Research International* 2025; **208**, 116269.

[50] FIS Masfufah, N Ngadiwiyana, Y Yassaroh, R Wulandari and NBA Prasetya. Antibacterial and pH-responsive chitosan/glutaraldehyde film with red cabbage anthocyanins for meat freshness detection. *Trends in Sciences* 2025; **22(9)**, 10254-10254.

[51] Z Akar, M Küçük and H Doğan. A new colorimetric DPPH• scavenging activity method with no need for a spectrophotometer applied on synthetic and natural antioxidants and medicinal herbs. *Journal of Enzyme Inhibition and Medicinal Chemistry* 2017; **32(1)**, 640-647.

[52] Z Bedlovičová, I Strapáč, M Baláž and A Salayová. A brief overview on antioxidant activity determination of silver nanoparticles. *Molecules* 2020; **25(14)**, 3191.

[53] I Best, S Casimiro-Gonzales, A Portugal, L Olivera-Montenegro, L Aguilar, AM Muñoz, L Aguilar, AM Muñoz and F Ramos-Escudero. Phytochemical screening and DPPH radical scavenging activity of 3 morphotypes of *Mauritia flexuosa* L.f. from Peru, and thermal stability of a milk-based beverage enriched with carotenoids from these fruits. *Heliyon* 2020; **6(10)**, e05209.

[54] A Sellam, Y Zerrouki, M Dali, A Maleb, I Khalid, N Hamdaoui, B Hammouti and M Meziane. *In vitro* antioxidant properties of *Lactobacillus gasseri* isolated from fermented milk: Isolation and Preparation of strains and intracellular cell-free extracts, chemical testing (hydrogen peroxide, superoxide, hydroxyl radical, DPPH, ferrous ion chelatin, and linoleic acid peroxidation. *The Indonesian Journal of Science and Technology* 2024; **9**, 611-622.

[55] E Genskowsky, LA Puente, JA Pérez-Álvarez, J Fernandez-Lopez, LA Muñoz and M Viuda-Martos. Assessment of antibacterial and antioxidant properties of chitosan edible films incorporated with maqui berry (*Aristotelia chilensis*). *LWT - Food Science and Technology* 2015; **64(2)**, 1057-1062.

[56] E Kusrini, K Nuzula, A Usman, LD Wilson, C Gunawan and AB Prasetyo. Enhanced cytotoxicity and antifungal effects of iron-oxide chitosan/samarium/ranitidine microparticles. *Sains Malaysiana* 2025; **54(1)**, 3673-3686.

[57] SB Schreiber, JJ Bozell, DG Hayes and S Zivanovic. Introduction of primary antioxidant activity to chitosan for application as a multifunctional food packaging material. *Food Hydrocolloids* 2013; **33(2)**, 207-214.

[58] J Jumina, D Siswanta, AK Zulkarnain, S Triono, Priatmoko, E Yuanita, AC Imawan, N Fatmasari and I Nursalim. Development of c-arylcalix[4]resorcinarenes and c-arylcalix[4]pyrogallolarenes as antioxidant and UV-B protector. *Indonesian Journal of Chemistry* 2019; **19(2)**, 273-284.

[59] MP Desai, RV Patil and KD Pawar. Green biogenic approach to optimized biosynthesis of noble metal nanoparticles with potential catalytic, antioxidant and antihaemolytic activities. *Process Biochemistry* 2020; **98**, 172-182.

[60] W Sun, B Karmakar, HA Ibrahium, NS Awwad and AF El-kott. Design and synthesis of nano Cu/chitosan-starch bio-composite for the treatment of human thyroid carcinoma. *Arabian Journal of Chemistry* 2022; **15(1)**, 103465.

[61] G Shu, D Xu, S Xie, LJ Chang, X Liu, J Yang, Y Li and X Wang. The antioxidant, antibacterial, and infected wound healing effects of ZnO quantum dots-chitosan biocomposite. *Applied Surface Science* 2023; **611**, 155727.

[62] N Almayda, NP Arraihan, D Alfira, M Masruri, E Susanti and A Safitri. Phytochemical compositions, microencapsulation, and antioxidant activity of aqueous extract from *Tithonia diversifolia* leaves. *Trends in Sciences* 2025; **22(9)**, 10306.

Supplementary Material

Antibacterial Performance of Nickel Chitosan Nanocomposites on Gram-Positive Bacteria

Figure S1 shows the antibacterial performance analysis of chitosan, nanoparticle chitosan, Ni@CS-5 to Ni@CS-25 nanocomposites, positive control (chloramphenicol) and negative control (CH_3COOH 2%) against gram-positive bacteria, specifically *S. pyogenes* ATCC 19615 (**Figure S1**), and *B. cereus* ATCC 10556 (**Figure S2**).

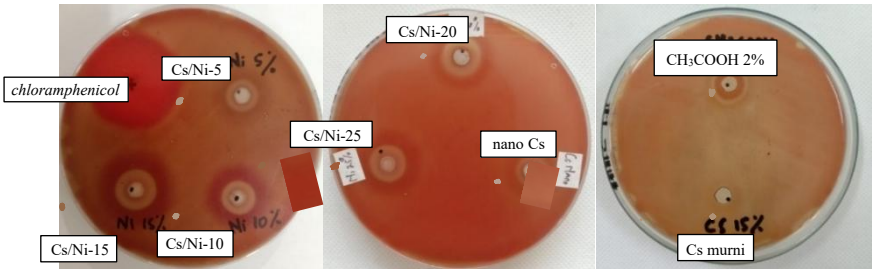

Figure S1 Antibacterial performance against *S. pyogenes* bacteria.

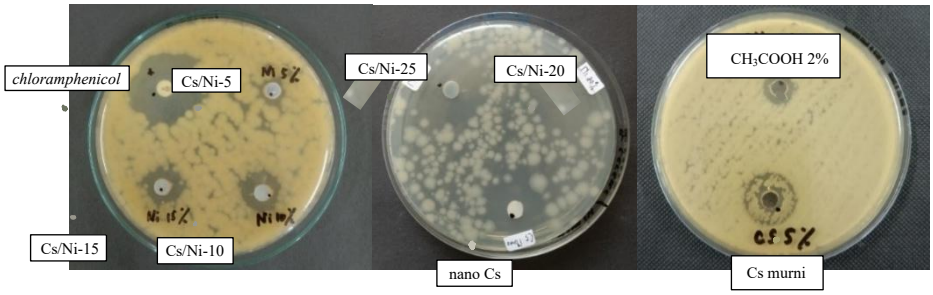

Figure S2 Antibacterial performance against *B. Cereus* bacteria.

Antibacterial Performance of Nickel Chitosan Nanocomposites on Gram-Negative Bacteria

Figure S1 shows the antibacterial performance analysis of chitosan, nanoparticle chitosan, Ni@CS-5 to Ni@CS-25 nanocomposites, positive control (chloramphenicol) and negative control (CH_3COOH 2%) against gram-negative bacteria, specifically *K. pneumoniae* ATCC 13883 (**Figure S3**) and *E. coli* ATCC 25922 (**Figure S4**).

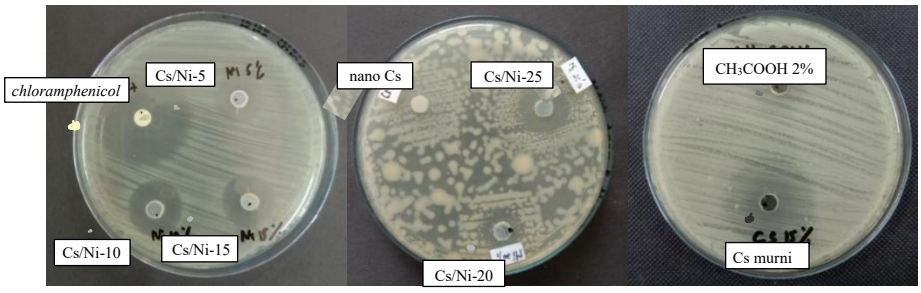

Figure S3 Antibacterial performance against *K. pneumoniae* bacteria.

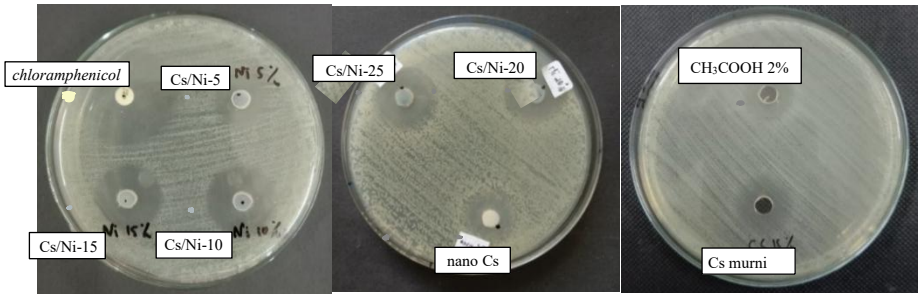

Figure S4 Antibacterial performance against *E. coli* bacteria.